Electron-neutrino selection and reconstruction in the MicroBooNE LArTPC using the Pandora multi-algorithm pattern recognition

The MicroBooNE collaboration

July 9, 2018

MICROBOONE-NOTE-1038-PUB

MicroBooNE (the Micro Booster Neutrino Experiment) is a liquid argon time-projection chamber experiment designed for short-baseline neutrino physics, currently running at Fermilab. It aims to address the anomalous excess of low-energy events observed by the MiniBooNE experiment. In this note we present a fully automated event selection algorithm to identify charged-current electron neutrino event candidates with no pions and at least one proton in the final state (ν_e CC0π-Np). The efficiency of the current selection algorithm is (46.5$\pm$0.3) %. We also show some cuts on kinematic and geometric variables which reject background events. These cuts have been validated by analyzing two event samples orthogonal to our signal. Future improvements have been identified which will improve the reconstruction efficiency, especially at low energy.

Contents

1 Introduction

One of the main physics goals of the MicroBooNE experiment is to clarify the nature of the low-energy excess of ν_e-like events observed by the MiniBooNE experiment in 2009 [1].

However, the MiniBooNE detector was a Čerenkov detector, which does not have the ability to distinguish between single electrons and single photons in the final state, making it very challenging to identify a physics model that could definitely explain the excess.

The MicroBooNE detector, a liquid argon time projection chamber (LArTPC), provides detailed tracking and calorimetry, which allows for powerful electron/photon identification. A detailed description of the detector is available in [2].

In this note we will describe a fully automated ν_e event selection in the MicroBooNE detector for the Booster Neutrino Beam (BNB) at the Fermi National Accelerator Laboratory.

2 Signal definition

The MiniBooNE experiment showed an excess of CCQE-like events in the 200-475 MeV neutrino energy range [1], therefore this analysis will focus on a similar topology.

Our selection aims to have a sample with one electron, no other leptons or photons, at least one proton, and no other charged hadrons or mesons in the final state. These events are called ν_e CC0π-Np (where N > 0) [3].

In MicroBooNE, a ν_e CC0π-Np interaction corresponds to one or more ionization tracks, produced by the protons, and an electromagnetic shower, produced by the electron.

3 Analysis Methodology

Charged particles traversing the TPC leave traces of ionization electrons, which are drifted to the anode, composed of the three wire planes. The planes have 3 mm wire spacing at angles of $+60°$, $-60°$, and $0°$ with respect to the vertical. The first two planes are referred to as *induction planes* and the wire plane furthest from the cathode is referred to as the *collection plane*. The planes are separated by 3 mm. Signal processing and noise suppression are extensively described in [4]. The waveforms observed on each wire are examined and a hit-finding algorithm searches for local maxima and minima. A Gaussian distribution is fitted to each peak and hits are created. The hits are input to the Pandora multi-algorithm pattern recognition software [5] which first runs a two-dimensional reconstruction in which hits are clustered together by a series of algorithms in each readout plane. The common coordinate to all three images is exploited by further algorithms to correlate features and perform three-dimensional reconstruction, identifying the 2D clusters that represent individual particles, and creating with them the final TPC reconstructed objects [6]. Further characterization of these objects will present them as track-like or shower-like based on topological features.

MicroBooNE also benefits from an optical detection system, comprised of 32 photomultipliers tubes placed behind the anode plane, with a few-ns timing resolution. They detect the argon scintillation light produced by the neutrino interaction and it provides the TPC start time of the event. Figure 1 shows a simulated ν_e CC0π-Np event display of the collection plane with an electron and two protons in the final state, and the corresponding reconstructed shower and reconstructed tracks. In this case, the algorithm is able to correctly identify the electromagnetic shower and both proton tracks.
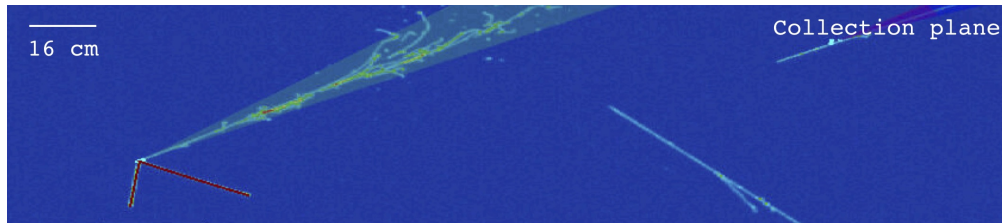
Figure 1: Monte Carlo ν_e CC0π-Np event display of the collection plane with an electron and two protons in the final state. The reconstructed shower-like object is represented by the green cone. The reconstructed track-like objects are represented by the red lines. The blue tracks are cosmic ray muons crossing the event. The color scale is proportional to the amount of charge collected by the wires.

3.1 Data and Monte Carlo samples

In this note we will analyze a subsample of the data collected by the detector between February and April 2016. This subsample corresponds to an exposure of the MicroBooNE detector of 4.4×10^{19} POT. This is MicroBooNE's unblinded sample for reconstruction, event selection development, and performance measurement. The sample is statistically too small to be sensitive to a MiniBooNE-like low-energy excess signal. The entire dataset will be open once the we are satisfied with the reconstruction, analysis chain, and future sensitivity estimates.

The data was collected in two different modes, obtaining two different samples:

Data on-beam. Each event was triggered in the detector by a flash in the optical detection system during the beam gate window, with the beam on;

Data off-beam. Each event was triggered in the detector by a flash in the optical detection system during an artificial beam gate window in which the beam is actually off. This sample is used to evaluate the *cosmic in-time* background, described in Section 3.7.

Two different Monte Carlo samples were produced:

ν_e **CC0π-Np + cosmic sample.** Each event has a simulated ν_e CC0π-Np interaction in the MicroBooNE cryostat and simulated cosmic rays hitting the detector in the same readout window;

BNB + cosmic sample. Each event has a simulated ν interaction, where the neutrino flavors are weighted according to the BNB neutrino flux composition, and simulated cosmic rays hitting the detector in the same readout window.

Neutrino events have been generated using the GENIE Neutrino Monte Carlo generator version 2.8.6 [7] and cosmic rays have been generated using the CORSIKA Monte Carlo generator version 7.4003 [8]. Simulated secondary particle propagation utilizes GEANT version 4.9.6 [9], and detector response simulation and reconstruction employs LArSoft version 6.26.01.10 [10].

3.2 Overview

The reconstruction and selection chain to identify ν_e CC0π-Np electron neutrino candidate events for this analysis is divided into several stages:

1. Cosmic-ray removal: in order to suppress the cosmogenic background [11, 12], two different Pandora reconstruction paths run with different sets of algorithms [5], a first one optimized for the reconstruction of cosmic-ray muons, and a second one optimized for the reconstruction of neutrino interactions. In between both reconstruction paths, hits associated to objects deemed as cosmic-induced by several tagging algorithms, external to Pandora and described in [13], are removed from the event. The remaining hit collection provides the input to the Pandora neutrino reconstruction path, which outputs a list of candidate neutrinos.

2. Optical pre-cuts and flash-matching: a minimum amount of coincident photoelectrons in the optical detection system is required and at least one of the neutrino candidates provided by the Pandora framework must be compatible with the flash in the optical detection system.

3. Electron neutrino topological pre-selection: one of the neutrino candidates must be compatible with the topology of a ν_e CC0π-Np interaction. Rather than accepting strictly N tracks and one shower, at least one track and at least one shower or at least two showers sharing a common vertex are accepted, due to the presence of split showers and split tracks. Multiple showers without reconstructed tracks are accepted due to a current track/shower identification inefficiency.

4. CC ν_μ neutrino candidates removal: events tagged as CC ν_μ neutrino candidates are rejected by a separate selection module [13].

5. Background rejection through calorimetric, kinematic, and geometric cuts: ν_e CC0π-Np events can be further isolated by applying a suite of cuts on kinematic, geometric, and calorimetric variables. The electromagnetic showers initiated by an electron in the final state are isolated with a cut on the dE/dx value and the proton tracks are selected with a Boosted Decision Tree (BDT) trained on the track dQ/dx and its length.

6. Energy spectrum reconstruction: the energy of the electron showers is measured with a calorimetric procedure, converting the collected charge into deposited energy, while the energy deposited by the proton tracks is calculated from the length of the reconstructed track.

3.3 Optical Detection System Selection

The optical selection serves two purposes: (1) it ensures that the optical flash which triggered the detector readout is compatible with the neutrino candidates from the Pandora neutrino-optimized reconstruction pass, and (2) it provides a way to discriminate between multiple Pandora neutrino candidate objects (most of which are of cosmic origin) by selecting the one most compatible with the flash in the optical detection system in time with the beam gate window.

The optical selection algorithm consists of three major stages:

1. cuts applied to optical properties of the reconstructed flash object (number of photoelectrons an TPC charge/PMT photoelectrons ratio);

2. cuts on the compatibility of the reconstructed flash with the Pandora neutrino candidate (position of the flash compared with the position of the center of the collected charge);

3. the Pandora neutrino candidate which is most compatible with the flash is picked using a likelihood method.

The effects of the optical selection have been studied in detail using the ν_e CC0π-Np + cosmic Monte Carlo sample.

3.4 Electron Neutrino Topological Pre-Selection

A perfectly reconstruction of a ν_e CC0π-Np event in a LArTPC will produce as many reconstructed tracks as the number of protons above the detection threshold in the final state and a single reconstructed shower (the electron), sharing a common vertex. However, mis-reconstruction and mis-classification can significantly lower the selection efficiency. The current status of the event reconstruction, which depends on the quality of the event (e.g. the number of hits [5]), affects the efficiency of selecting these events. For example, the presence of dead or unresponsive wires can damage the reconstruction by causing the splitting of an ionization track or an electromagnetic shower into two distinct reconstructed object. Also, the selection currently implemented relies on the classification of the reconstructed objects as track-like or shower-like, separation that contains an inherent inefficiency associated, specially when the number of reconstructed hits is low.

In order to maximize our efficiency we currently require (1) *at least* one track and *at least* one shower sharing a common vertex, or (2) *at least* two showers sharing a common vertex, to account for proton misclassification as a shower-like object. For these cases we run additional bi-dimensional Principal Component Analyses in the collection plane among the reconstructed shower-like objects, to ensure that a mis-classified shower is compatible with a track. The object with the largest first eigenvalue is chosen as the proton track candidate and it is then considered as a track-like object. This particular step is only a temporary solution as the Pandora framework is being adapted to improve these cases.

3.5 Minimum quality requirements

A minimal set of cuts is applied to the selected events, in order to ensure that they are well reconstructed. First, to avoid border effects, the reconstructed neutrino vertex, the start point of the reconstructed showers and the start and end points of the reconstructed tracks are required to lie within a fiducial volume. Our fiducial volume cut is 10 cm from each side on the x axis, 20 cm from each side on the y axis, and 10 cm (50 cm) from the upstream (downstream) side on the z axis. Since electromagnetic showers develop mainly in the forward direction with respect to the beam, the asymmetric cut on the z axis (which corresponds to the beam direction) helps reject non-fully contained events which begin too close to the downstream end of the TPC. We also require, for each event, (1) at least 5 hits in the collection plane associated to a shower-like object, (2) at least 5 hits in the collection plane associated to a track-like object, and (3) at least one hit in every plane.

3.6 Selection efficiency

The selection efficiency of our algorithm is obtained by calculating the fraction of events selected in the ν_e CC0π-Np + cosmic Monte Carlo sample, with a true neutrino vertex in the fiducial volume.

In order to understand what energy thresholds are appropriate for reconstruction in the TPC, dedicated studies have been performed on proton tracks and electron showers, using the ν_e CC0π-Np + cosmic Monte Carlo sample. We have found that we have no efficiency for reconstructing and classifying protons below 40 MeV and electrons below 20 MeV in ν_e CC0π-Np events following
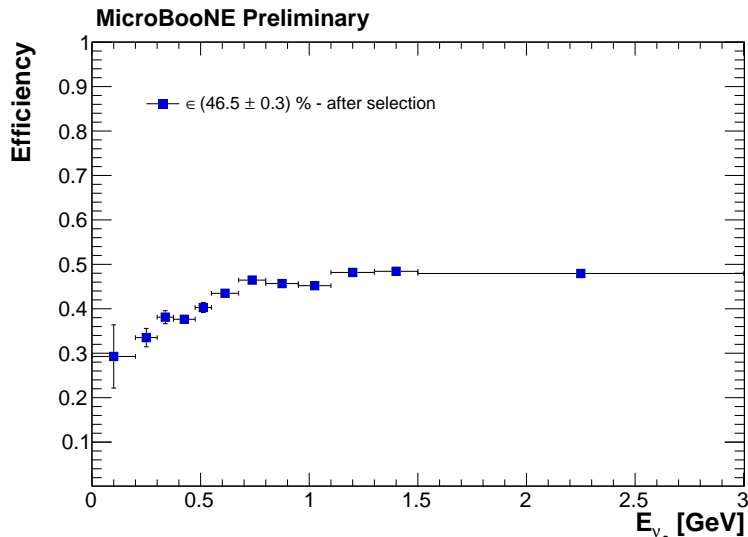
Figure 2: ν_e CC0π-Np selection efficiency as a function of the true ν_e energy. Each true proton in the final state is required to have a kinetic energy larger than 40 MeV and each true electron larger than 20 MeV.

these optical, topological, and minimum quality pre-selections. Therefore, these energy thresholds are applied to the simulations to allow a fair comparison with the reconstructed particles.

Our overall ν_e CC0π-Np selection efficiency ϵ is defined as:

$$\epsilon = \frac{\text{N. of selected CC0}\pi\text{-Np events}}{\text{N. of generated CC0}\pi\text{-Np events}}, \tag{1}$$

where each selected event must pass the optical selection and satisfy the topology and minimum quality requirements.

Figure 2 shows the efficiency as a function of the true neutrino energy. At this point, we do not attempt to estimate any systematic uncertainty: here and in the rest of the note the error bars represent statistical uncertainties only, both for data and Monte Carlo.

As expected, the efficiency increases with the neutrino energy, since high-energy events correspond in general to a larger number of hits in the TPC and the Pandora framework reconstruction performances increase with the number of reconstructed hits [6].

A description of future improvements, which will allow us to increase the selection efficiency, is included in Section 6.

3.6.1 Inefficiencies breakdown

Our current selection algorithm can fail for several reasons: in particular, we could have problems in the classification, such as an electron classified as a track-like object, or particles not reconstructed at all. We identified four main causes for our selection inefficiency, whose contributions have been estimated with the same simulated sample described in Section 3.6:

Mis-identfied background (not fully contained). We require the start and end points of the

track-like objects and the start point of the shower-like objects to be fully contained. However, we find events falsely reconstructed as contained, but the electron or the proton truly escape the the fiducial volume, especially at high energies. These events represent 8.0% of the total.

Mis-identified background (cosmic). When we have two or more neutrino interaction candidates, the flash-matching algorithm chooses the one most compatible with the hypothesis of a neutrino interaction. The compatibility is quantified by the likelihood of the flash hypothesis, built starting from the collected charge, with the measured flash in the optical system. However, in some cases, the wrong neutrino candidate is selected (*cosmic* background). These events are 9.0% of the total and they decrease the purity of the selected sample.

Mis-identified background (cosmic contaminated). The selected neutrino candidate has one or more reconstructed objects of cosmic origin that were wrongly attached to the neutrino interaction (*cosmic contaminated* background). These events are 18.5% of the total. Also in this case, this fraction affects the purity of our sample.

Not selected (reconstruction and classification issues). In these events the correct neutrino candidate is selected: however, the electron shower can be mis-classified as a track or the proton may not be reconstructed at all. These events represent 9.1% of the total.

Not selected (no flash/no candidates). A fraction of the generated events does not have a flash that satisfies our current optical requirements or does not have any neutrino candidate in the event. These events are 8.9% of the total.

Figure 3 shows a stacked histogram of the generated events, divided into the categories described above. The *correctly selected ν_e CC0π-Np* category corresponds to the efficiency plot shown in Figure 2.

3.7 Selection results

The previous selection efficiency results were performed with the ν_e CC0π-Np + cosmic sample. We now look at the selection performances when analyzing events coming from the BNB beam Monte Carlo simulation with cosmic rays in the same readout window (BNB + cosmic sample). In this case, the selected events will contain background events coming from beam and cosmic-ray events. We divide the selected events (signal and background) into 8 categories:

Beam intrinsic ν_e CC0π-Np: charged-current ν_e neutrino interaction with no pions in the final state, at least one proton with a kinetic energy larger than 40 MeV (N > 1), and an electron with a kinetic energy larger than 20 MeV. This category represents the signal of our analysis.

Beam intrinsic ν_e CC: charged-current ν_e neutrino interaction that is not ν_e CC0π-Np or where the electron or the protons were below the kinetic energy thresholds defined above.

Beam intrinsic ν_μ: charged-current ν_μ neutrino interactions.

Beam intrinsic NC: neutral current neutrino interaction (both ν_μ and ν_e).

Outside fiducial volume: neutrino interactions which occur in the liquid argon outside the fiducial volume, but with one or more final-state particles inside in the fiducial volume.
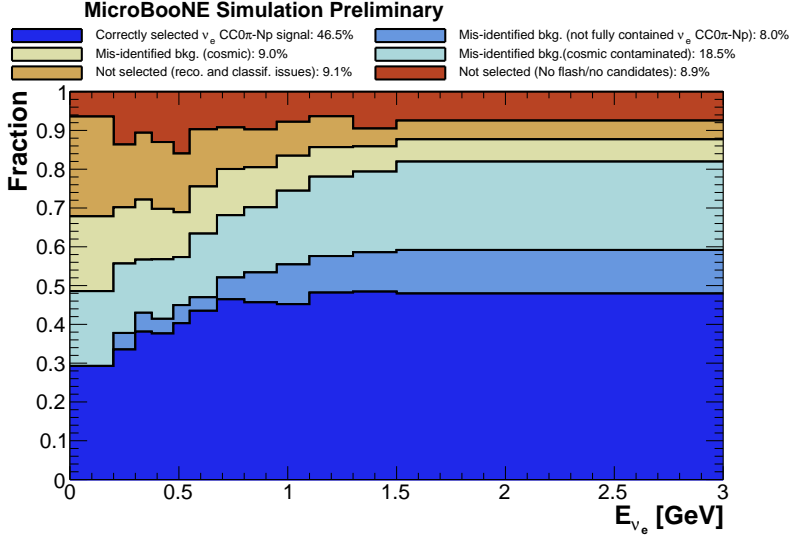
Figure 3: Stacked histogram of generated events as a function of the true neutrino energy, categorized into correctly identified signal events and different reconstruction or identification failure modes.

Cosmic contaminated a neutrino interaction candidate with at least a cosmogenic track or shower, attached to a correctly reconstructed neutrino candidate.

Cosmic in-time events with no neutrino interaction, but where a cosmic-ray interaction in time-coincidence with the beam spill triggered the event, and activity was selected as a neutrino candidate In order to evaluate the cosmic in-time background we use the *data off-beam* sample, as defined in Section 3.1.

Cosmic neutrino interaction in the event, but with selected cosmic-ray interaction happening during the same readout window and which interaction is chosen as the neutrino interaction.

Table 1 shows a summary of the selection algorithm results, with the corresponding number of events for each category.

A large fraction of the beam intrinsic ν_μ events are removed by rejecting the events selected by an external analysis [13], which looks for charged-current ν_μ candidates in the same data sample used here.

Figure 4 shows the reconstructed energy spectrum obtained rejecting the events that were flagged as CC ν_μ candidates by this external analysis. The reconstructed energy has been measured with the procedure described in Section 4. The ratio between the number of data events and the sum of the BNB + cosmic Monte Carlo and data off-beam events (normalized by the number of POT) is 1.01 and the value of the χ^2/n.d.f. (1.00) shows that the two distributions agree also in shape.

The agreement between data and simulation is also verified in the angular distributions of the most energetic shower-like objects, shown in Figure 5. As expected, the neutrino distributions are constant on the azimuthal angle ϕ and peaked at low inclination angle θ values, since the interactions are mostly forward going. The inclination angle θ distribution agrees well both for shape and normalization. The azimuthal angle ϕ distribution shows a slight disagreement around

Category	Generated	Selected	Efficiency
ν_e **CC0π-Np (signal)**	32.037 ± 0.005	14.919 ± 0.004	$(46.5 \pm 0.3)\%$
ν_e CC	32.821 ± 0.005	11.130 ± 0.003	$(34.3 \pm 0.2)\%$
Beam intrinsic ν_μ	10313.9 ± 2.0	841.2 ± 0.6	$(8.1 \pm 0.1)\%$
Beam intrinsic NC	3265.4 ± 1.1	310.3 ± 0.4	$(9.5 \pm 0.2)\%$
Outside fid. vol.	2595.1 ± 1.0	49.8 ± 0.1	$(1.9 \pm 0.2)\%$
Cosmic in-time	123070.2 ± 47.0	1045.3 ± 4.3	$(0.8 \pm 0.1)\%$
Cosmic contaminated	-	238.6 ± 0.3	-
Cosmic	-	226.7 ± 0.3	-

Table 1: Summary of the selection results, showing the contribution of each event category, for a MicroBooNE exposure of 4.4×10^{19} POT. Uncertainties are statistical only.
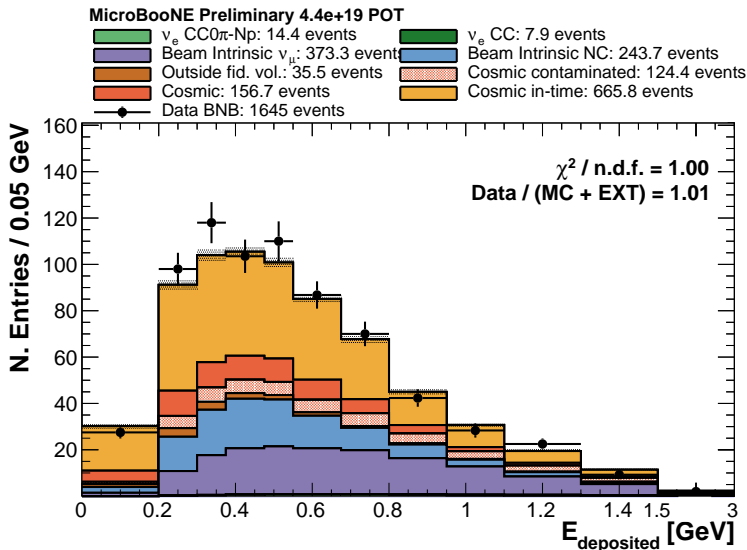
Figure 4: Reconstructed energy spectrum after the event selection algorithm and the veto of the events selected by the CC ν_μ module. The histograms of the event categories are stacked.

$\phi = 0°$ and $\phi = \pm 180°$. These differences were also observed in other analyses and they are likely to be attributed to imprecise signal simulation that predominantly affects tracks moving exactly towards or away from the anode [14, 15]. Work is ongoing to improve this and it will be addressed in a future simulation and reconstruction version.

(a) Inclination angle θ.
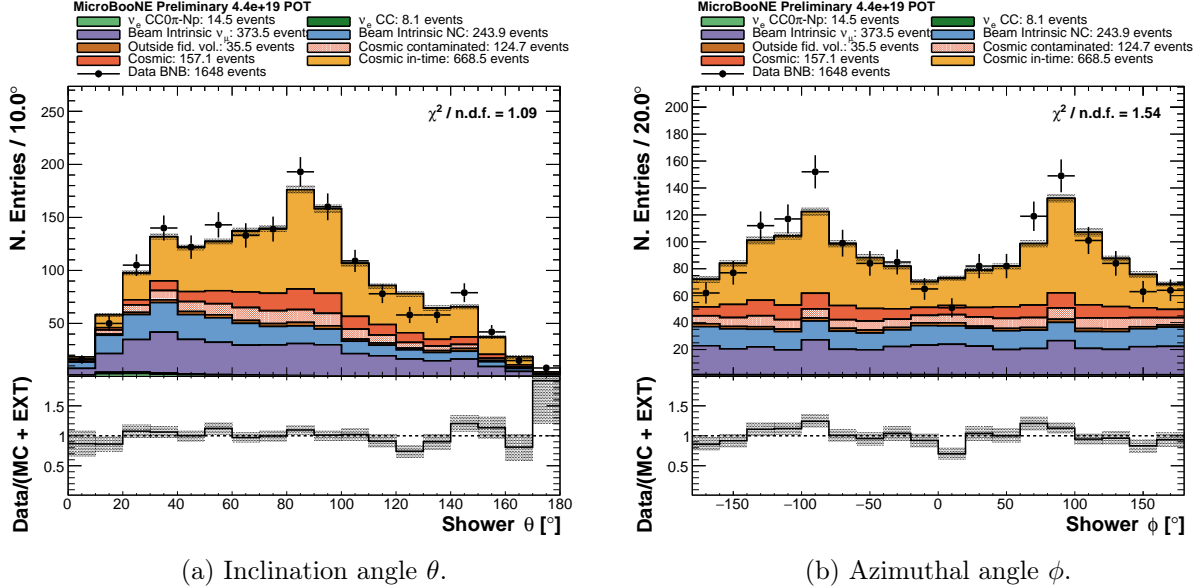
(b) Azimuthal angle ϕ.

Figure 5: Distributions of the azimuthal angle ϕ and the inclination angle θ of the most energetic shower after the CC ν_μ event rejection stage.

A small fraction of the data events were also visually inspected: Figure 6 shows three event displays of data events which contain a ν_e CC0π-Np event.

3.8 Background Rejection

In this section we will describe the cuts we could apply to our selected events, in order to isolate the ν_e CC0π-Np event candidates. The cuts have been chosen to (1) reduce the background, and (2) ensure that the selected events are well reconstructed. The values of each cut have been chosen manually to maximize the purity while retaining a sufficient efficiency.

3.8.1 Kinematic and calorimetric cuts analysis

In this section we will study all the variables used to apply the kinematic and calorimetric cuts. In particular, we will show, for each variable:

- the area-normalized Monte Carlo distributions for the signal (ν_e CC0π-Np events), the cosmogenic background (cosmic, cosmic contaminated, and cosmic in-time), and the neutrino background (ν_e CC, beam intrinsic ν_μ, beam intrinsic NC, and outside fid. vol.), to show the rejection power of each cut;

- the POT-normalized Monte Carlo and data distributions, to verify the agreement of the simulation with the collected data.

11
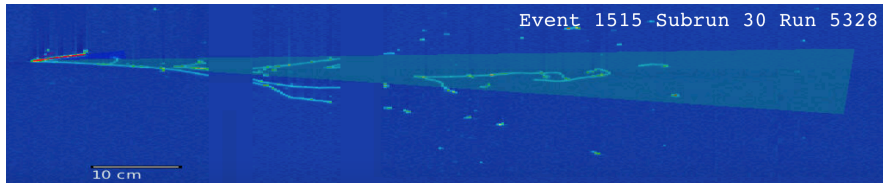
(a) Event 1515, Subrun 30, Run 5328
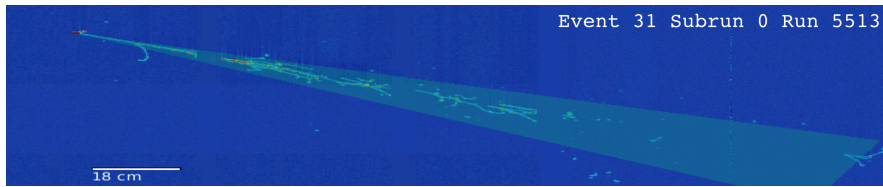
(b) Event 31, Subrun 0, Run 5513
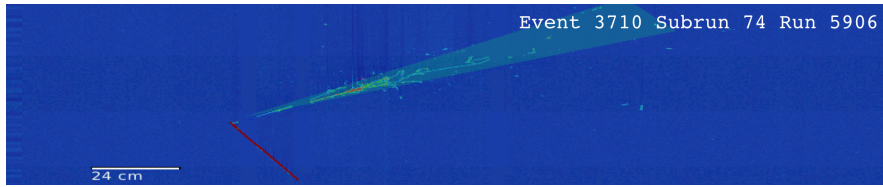
(c) Event 3710, Subrun 74, Run 5906

Figure 6: Event displays of the collection plane of three ν_e-like data events present selected by our algorithm. The gaps are caused by the presence of missing or unresponsive wires. The red lines correspond to reconstructed track-like objects and the green cones correspond to reconstructed shower-like objects.

Number of reconstructed hits > 50. A large number of cosmic-ray events may fake a neutrino candidate with a low number of hits. The area-normalized distributions in Figure 7a show that a large fraction of the cosmogenic backgrounds has a very low number of reconstructed hits in the collection plane, while the signal and the neutrino components have a much broader distribution. Figure 7b shows a good data/Monte Carlo agreement for this variable (χ^2/n.d.f. $= 1.28$).

Most energetic shower $E > 50$ MeV. The energy of each electromagnetic shower is measured with the procedure described in Section 4.2. A large number of cosmic in-time events will have a low shower energy, mainly caused by Michel electrons from stopping cosmic muons. A significant portion of charged-current ν_μ events will also have low-energy showers from Michel electrons from stopping muons and spurious hits. A cut of 50 MeV on the reconstructed energy (not corrected by the calibration factor measured in Section 4.2) of the most energetic shower removes a large fraction of the cosmic in-time and CC ν_μ backgrounds, without significantly reducing the ν_e CC0π-Np efficiency. However, this threshold could reduce our efficiency towards a low-energy excess of electron neutrino events and it will be replaced with more sophisticated algorithms in the future. The area-normalized distributions in Figure 8a show that a large fraction of the cosmogenic and neutrino backgrounds have very low-energetic showers, while the signal component is almost constant. Figure 8b shows a good data/Monte Carlo agreement for this variable (χ^2/n.d.f. $= 0.89$).

Most energetic shower 1 MeV/cm $< dE/dx < 3.2$ MeV/cm. The rate of energy loss per length (dE/dx) for electromagnetic showers is measured with a procedure analogous to the one described in [16]. All the hits of the collection plane within a rectangle of 4 cm along the direction of the shower and 1 cm perpendicular to the shower are collected. The dQ/dx for each hit is measured dividing the collected charge (dQ) by the pitch (dx) between each hit and the next one along the shower direction. The pitch corresponds to the distance in the TPC that a particle travels between its two projections on adjacent wires, which is *at least* the wire spacing (3 mm for MicroBooNE [2]). The dE/dx is calculated from the dQ/dx by using the calibration factor measured in Section 4.2, eq. (2). Since the distribution of the dE/dx hit values has an asymmetric tail due to the Landau nature of the process, we assign to the shower the median (and not the mean) of the dE/dx hit distribution. Figure 9a shows that the signal distribution is peaked around 2 MeV/cm, as expected. The peak around 0 MeV/cm is caused by showers with a low number of associated hits, or where the shower was mostly aligned with the wires of the collection plane (having as such a high pitch value). The beam intrinsic NC component has a second peak around 4 MeV/cm, mainly caused by $\pi^0 \to 2\gamma$ decays. Thus we apply the cut 1 MeV/cm $< dE/dx < 3.2$ MeV/cm, around the electron peak. The POT-normalized plot (Figure 9b) shows a very good data/Monte Carlo agreement (χ^2/n.d.f. $= 1.02$).

Proton track BDT score > 0.1. The aim of the analysis is to find ν_e CC0π-Np events. As such, it is necessary to identify and reject events with non-proton tracks in the final state (e.g. pions and muons). A boosted decision tree (BDT) has been trained using the length of the track and its dQ/dx using the TMVA toolkit version 4.2.1 [17]. The dQ/dx of the track has been calculated by taking the median of the dQ/dx hits distribution. The training sample is a simulated dataset of BNB neutrino interactions with cosmic rays. The signal is defined as all the fully-contained reconstructed tracks produced by protons and the background as all the

13

fully-contained reconstructed tracks produced by muons. Figure 10a shows the BDT score for the tracks in background and signal events. The cut at 0.1 allows to remove events with muon-like tracks. Low BDT score for signal events is caused by showers mis-reconstructed as track-like objects. The data/Monte Carlo agreement shown in Figure 10b is good both in the signal region (high score) and in the background region (low score). This cut is temporary as a more powerful particle identification algorithm is currently under development.

Track distance $d_t < 5$ cm. A well reconstructed event with a proton in the final state will have a reconstructed track attached to the reconstructed neutrino vertex. This conservative cut can be tightened as understanding of the spatial resolution improves. The most proton-like track, chosen using the score assigned by the proton BDT, is required to be within 5 cm of the reconstructed neutrino vertex. Figure 11a shows that the distributions of the distance between the start point of the most proton-like track and the reconstructed neutrino vertex for signal and background are very similar. The cut $d_t < 5$ cm, then, mainly ensures that the event is well reconstructed.

Shower distance $d_s < 5$ cm. Liquid argon TPCs such as MicroBooNE can distinguish between photons and electrons in two ways: (1) measuring the dE/dx of the start of the electromagnetic shower, and (2) measuring the gap between the interaction vertex and the start of the electromagnetic shower. In fact, photons produced in the final state of the neutrino interaction can travel several centimeters without interacting. In order to suppress events with a photon in the final state, the most energetic shower starting point is required to be within 5 cm of the reconstructed neutrino vertex. Figure 12a shows the distributions of the distance between the start point of the most energetic shower and the reconstructed neutrino vertex for signal and background events. As expected, background neutrino events have a slightly larger tail than the signal events. The agreement between data and Monte Carlo shown in Figure 12b is good. Improvements currently implemented in the Pandora framework will allow for more appropriate cuts to further reduce the photon background.

Track-shower angle $\cos\alpha > -0.9$. Electrons often start producing an appreciable shower in the detector after several centimeters. As such, the reconstruction framework identifies the first part of the shower as a track-like object and the latter part of the shower as a shower-like object. Furthermore, high-energy cosmic rays can produce a shower in the detector, which will be mostly aligned to a cosmic muon track. In order to remove these mis-reconstructed events and reduce this kind of cosmogenic background we require $\cos\alpha > -0.9$, where α is the angle between the most energetic shower and the most proton-like track, as identified by the proton BDT. Figure 13a shows that there are, in proportion, more background events for events with a high angular separation between the most proton-like track and the most energetic shower. This cut allows to reject these events while also ensuring that the signal events are well-reconstructed. In fact, signal events with $\cos\alpha \approx -1$ have almost always an electron shower reconstructed as a track-like object in the first part. The agreement shown in Figure 13b is good. Future improvements to the shower reconstruction will allow for an increased selection efficiency.

Most energetic shower opening angle $1° < \beta < 20°$. Reconstructed showers corresponding to electrons will have in general a small opening angle β. Requiring the most energetic shower to be smaller than $20°$ and larger than $1°$ allows to reduce the background component without

significantly impacting the signal efficiency. In this way we are able to reject ν_μ events and showering cosmic-ray events, which have on aveger opening angles. The requirement on the minimum value of the opening angle allows also to reject events with tracks mis-reconstructed as shower-like objects. The distributions of the opening angle β of the most energetic shower for neutrino and cosmic background events have a larger tail than the signal events, as shown in Figure 14a. The cut $1° < \beta < 20°$ helps rejecting some background events, while removing only a small fraction of mainly high-energy signal events. Figure 14b shows a good data/Monte Carlo agreement.

Longest track length $L < 80$ cm . Our signal sample will contain only protons in the final state. Protons in liquid argon have a higher stopping power than muons, which will correspond on average to shorter tracks. Each reconstructed track in the selected sample is required to be shorter than 80 cm. This cut helps rejecting mainly CC ν_μ events with high-energy muons in the final state. Both neutrino and cosmic background events have on average longer reconstructed tracks than signal events, as shown in Figure 15a. The cut $L < 80$ cm increases the signal purity without significantly decreasing the signal efficiency. The agreement between data and Monte Carlo distributions is good (Figure 15b). A dedicated particle identification algorithm currently under development will replace this cut in the future.

(a) Area normalized.   (b) POT normalized.
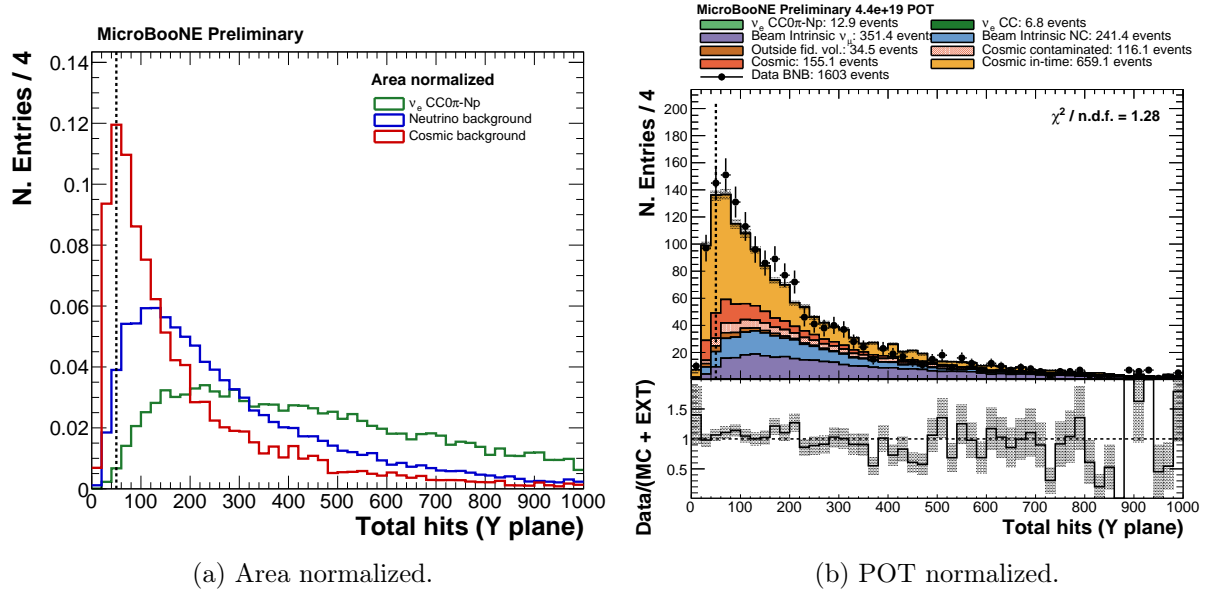
Figure 7: Area and POT normalized distributions of the number of reconstructed hits in the collection plane for all objects per event.

(a) Area normalized.
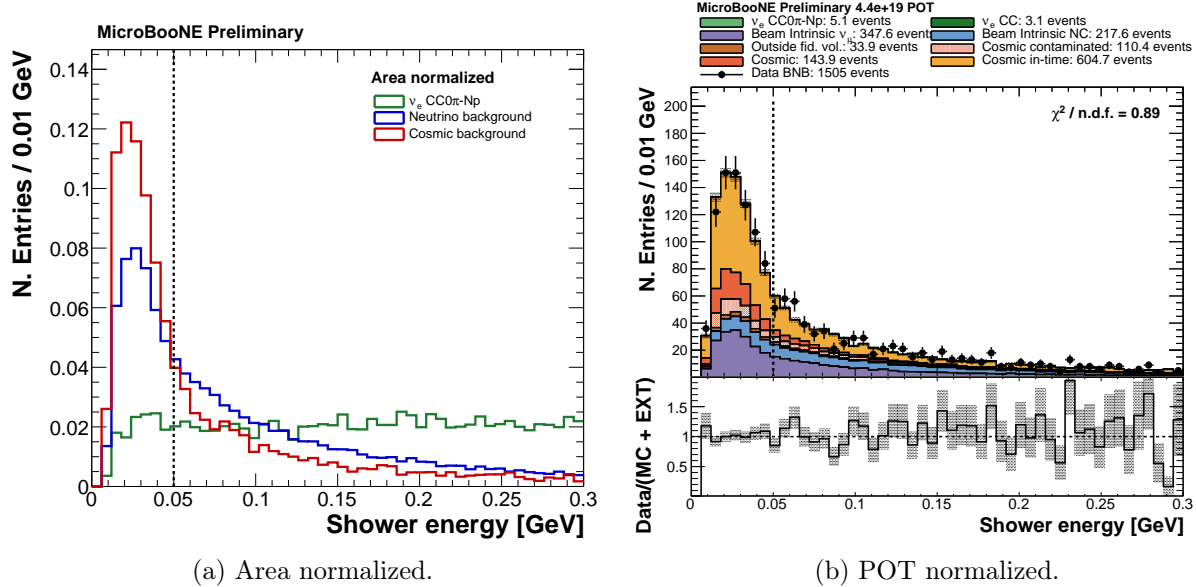
(b) POT normalized.

Figure 8: Area and POT normalized distributions of the energy of the most energetic shower.

(a) Area normalized.
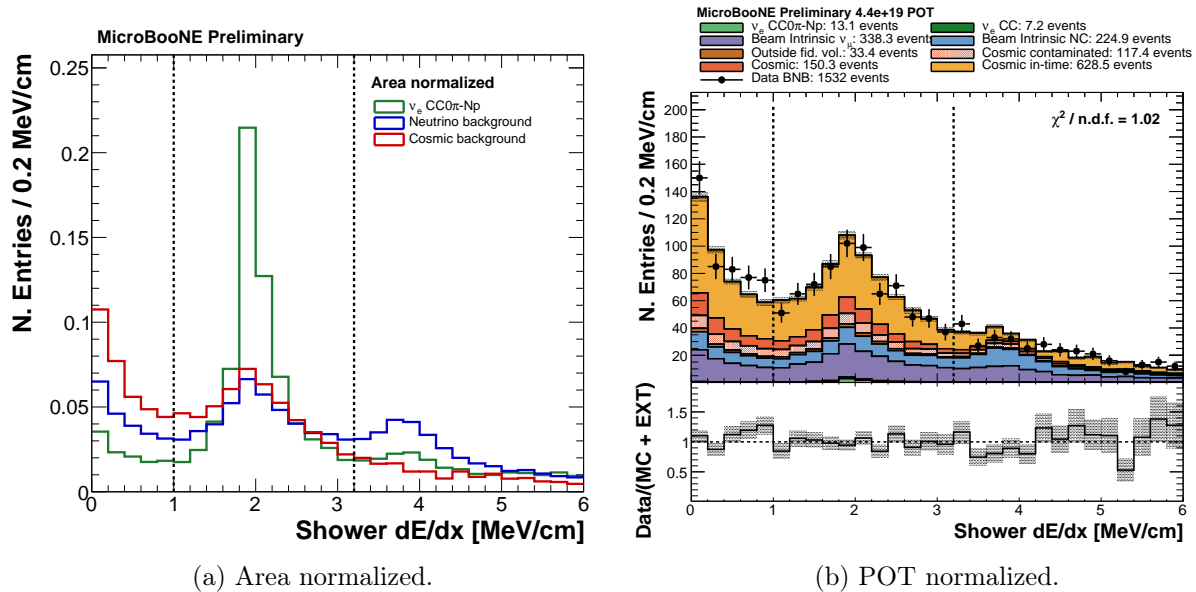
(b) POT normalized.

Figure 9: Area and POT normalized distributions of the dE/dx of the most energetic shower.

(a) Area normalized.
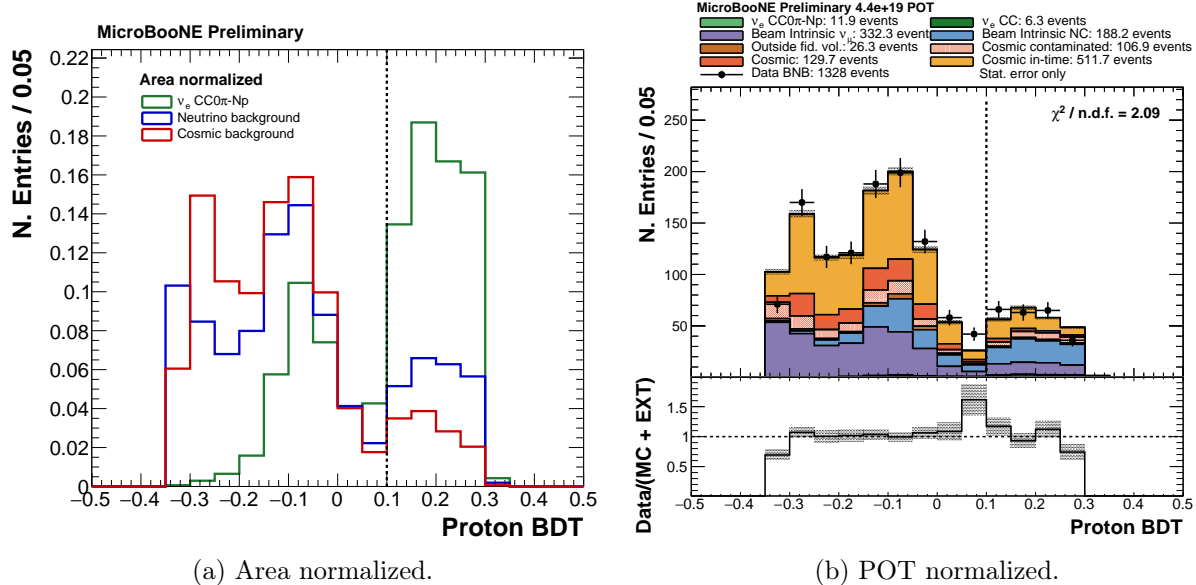
(b) POT normalized.

Figure 10: Area and POT normalized distributions of the highest BDT score in the event.

(a) Area normalized.
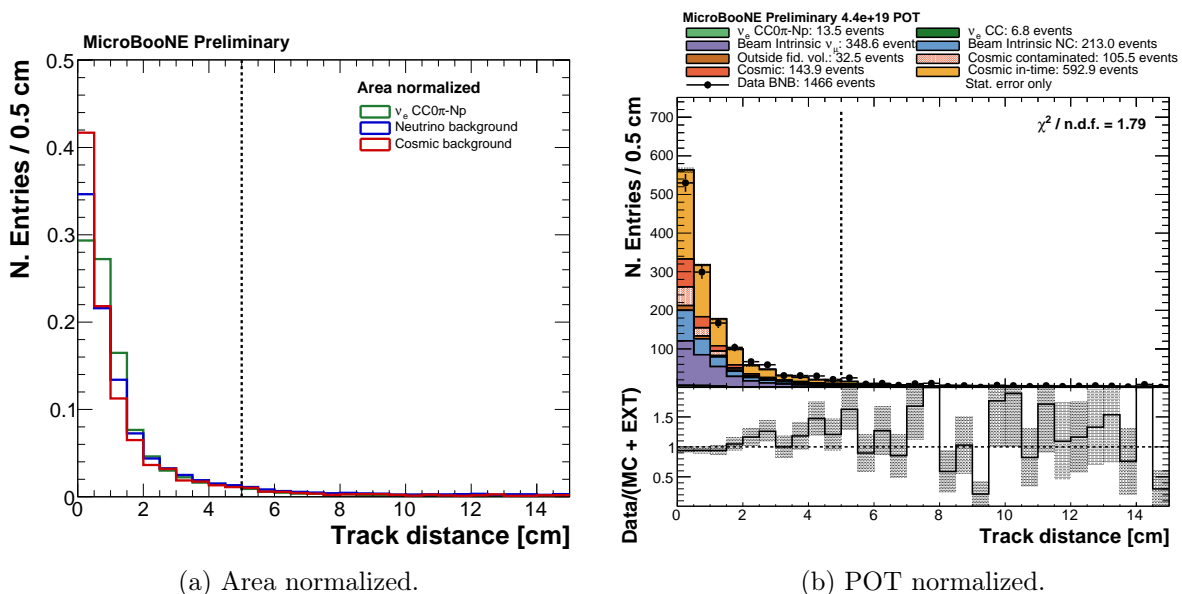
(b) POT normalized.

Figure 11: Area and POT normalized distributions of the distance between the most proton-like track, selected with the proton identification BDT, and the reconstructed neutrino vertex.

(a) Area normalized.
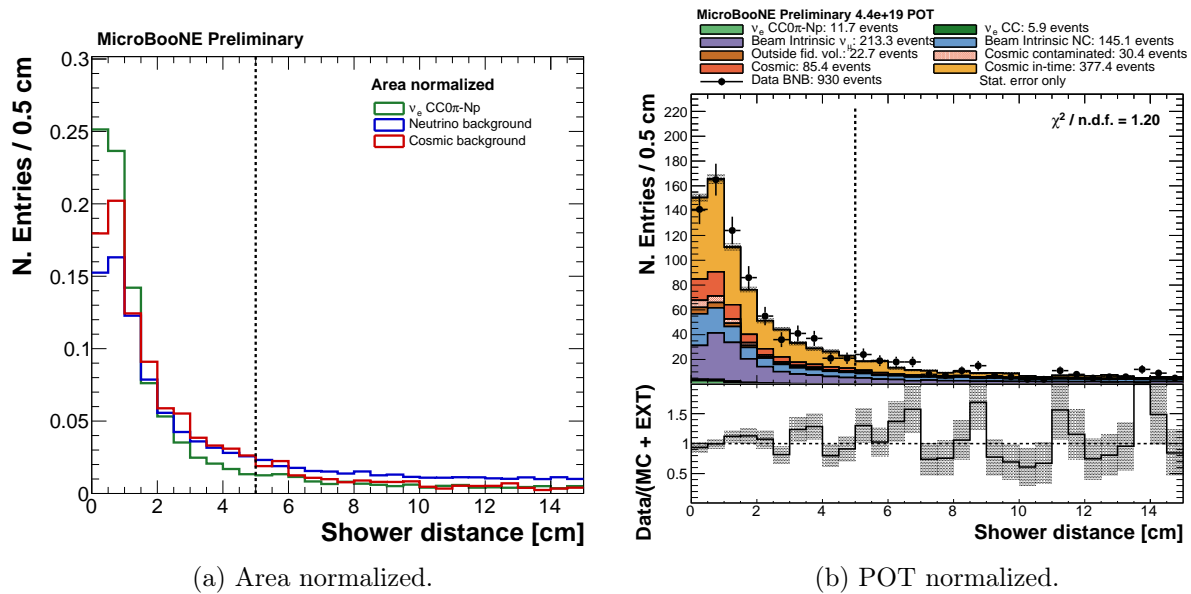
(b) POT normalized.

Figure 12: Area and POT normalized distributions of the distance between the most energetic shower and the reconstructed neutrino vertex.

(a) Area normalized.
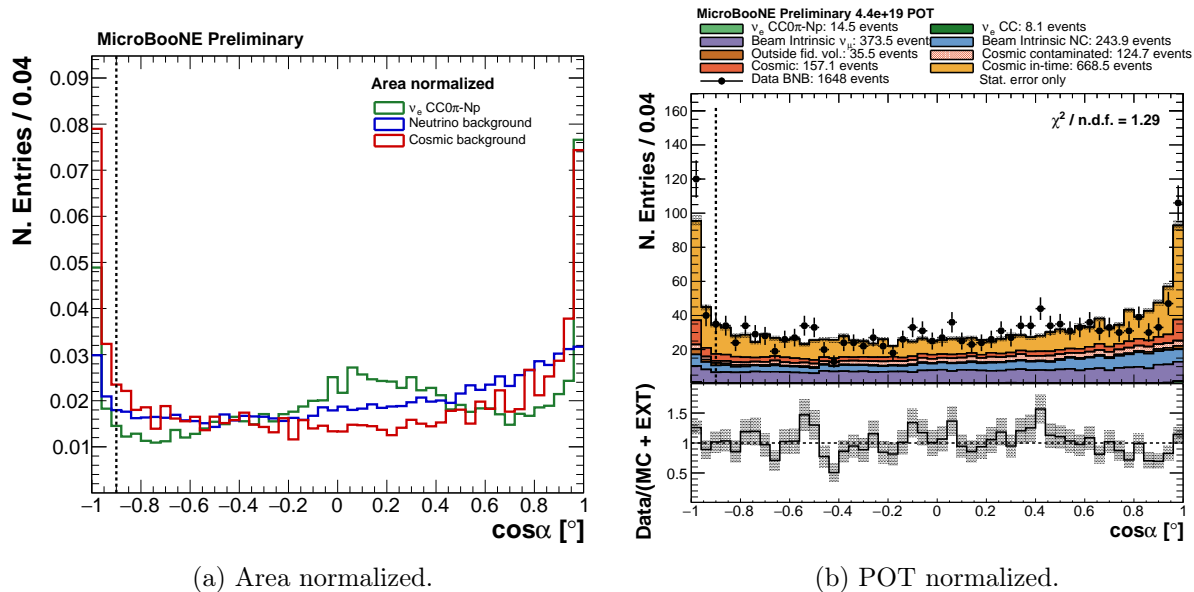
(b) POT normalized.

Figure 13: Area and POT normalized distributions of the angle α between the most proton-like track, selected with the proton identification BDT, and the most energetic shower.

(a) Area normalized.
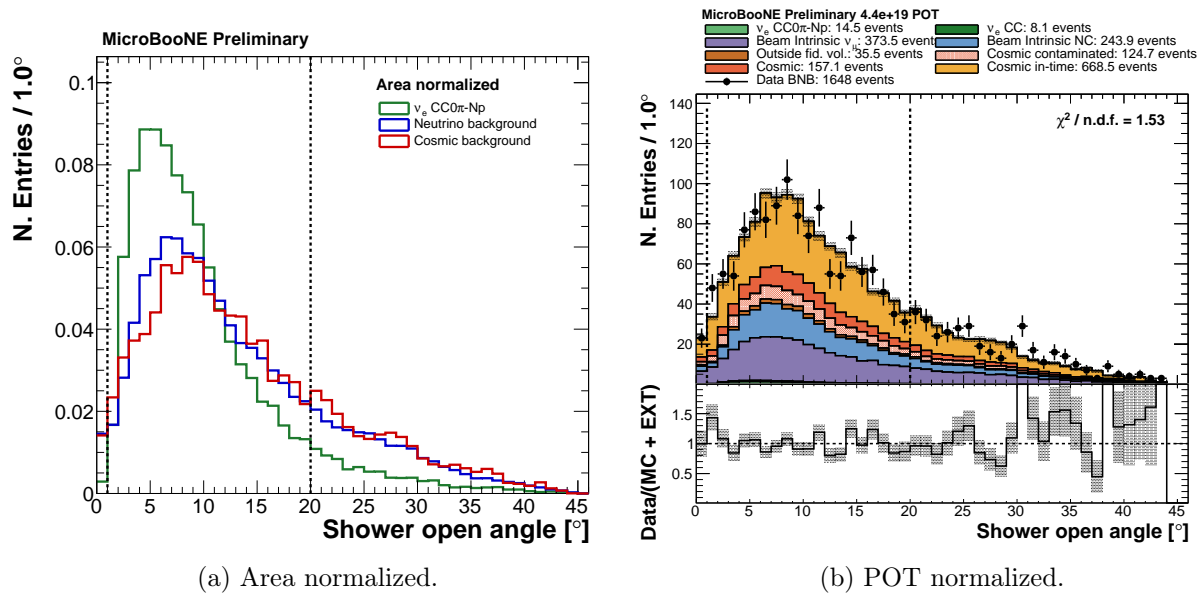
(b) POT normalized.

Figure 14: Area and POT normalized distributions of the opening angle β of the most energetic shower.

(a) Area normalized.
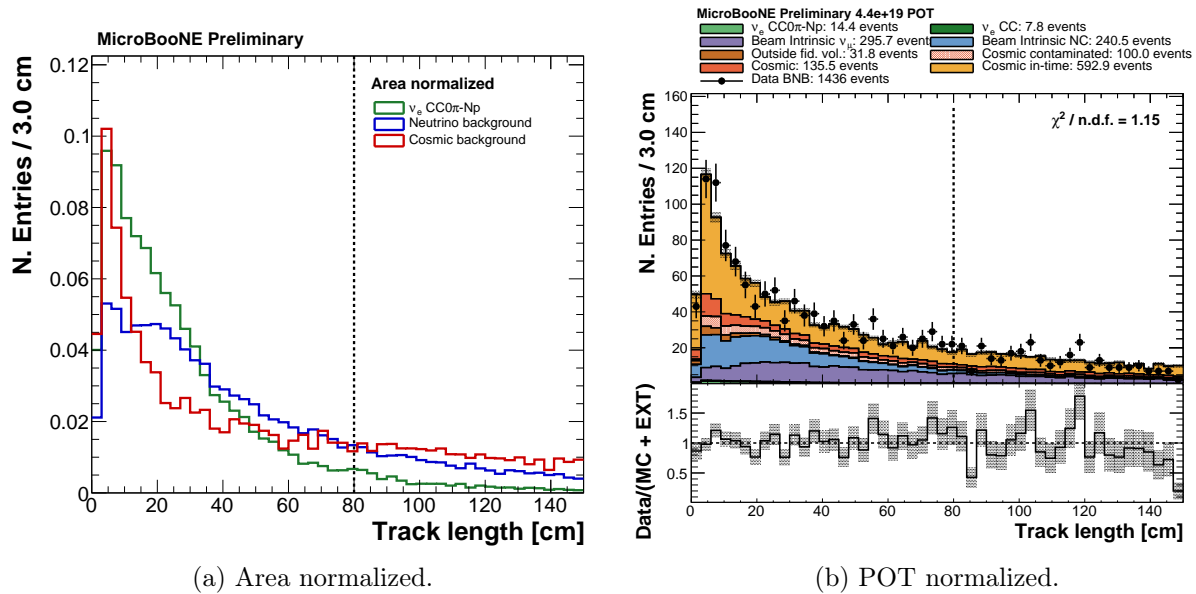
(b) POT normalized.

Figure 15: Area and POT-normalized distributions of the length of the longest track in the event.

4 Energy reconstruction

4.1 Scope of the energy reconstruction

In this analysis we restrict ourselves to the measurement of the deposited energy in the TPC of the visible particles in the final state of the neutrino interaction. Our signal will have in its final state, by definition, one electron and at least one proton, with no other visible particles. The energy of the electron will be measured by converting the reconstructed charge of all the shower-like objects into deposited energy, as described in Section 4.2. The energy of the protons, instead, can be measured by converting the track length of the reconstructed tracks into deposited energy, using the tabulated stopping power of protons in the liquid argon, with the procedure described in 4.3. The total reconstructed energy will correspond to the sum of the reconstructed energies, corrected by the calibration factors calculated below, and will be referred to as $E_{deposited}$.

4.2 Electron energy reconstruction and calibration

The reconstructed energy E_{reco}^e of a shower-like object is measured converting the charge of the associated hits into deposited energy in the TPC. It is calculated by multiplying the reconstructed charge (e_{reco}^-) from hits associated with the reconstructed shower by the calibration factor [18]:

$$\frac{E_{reco}^e(\text{MeV})}{e_{reco}^-} = 1.01 \frac{e^-}{e_{reco}^-} \times \frac{23.6 \text{ eV}}{e^-} \times 10^{-6} \frac{\text{MeV}}{\text{eV}} \times \frac{1}{R}, \tag{2}$$

where:

- the correction factor $1.01 \frac{e^-}{e_{reco}^-}$ is obtained measuring the true number of collected electrons e^- on the wires using a sample of stopping muons, fitting the dE/dx vs. residual range to values for argon as tabulated by the PDG [19];

- $\frac{23.6 \text{ eV}}{e^-}$ is the work function for ionizing an argon atom [20];

- $R = 0.62$ is the recombination factor obtained with the Modified Box Model [21] at Micro-BooNE's electric field of 270 V/cm.

The reconstructed energy is obtained summing the energy of each hit from the reconstructed showers produced by a simulated electron in the collection plane, produced by a ν_e CC0π-Np interaction. The starting point of the simulated electron and the starting point of the reconstructed showers are required to be within the fiducial volume. Since the reconstructed energy distributions in each true energy bin are asymmetric, the data points are obtained fitting a Gaussian around the peak of the distribution, in order to estimate the most probable value. Figure 16 shows the calibration slope necessary to convert the electron reconstructed energy E_{reco}^e into true electron energy E^e.

A linear fit of the data points gives:

$$E_{reco}^e = 0.78 \ E^e - 0.02 \text{ GeV}. \tag{3}$$

The energy of the shower, corrected by the calibration factor is then defined as:

$$E_{deposited}^e = (E_{reco}^e + 0.02 \text{ GeV})/0.78. \tag{4}$$
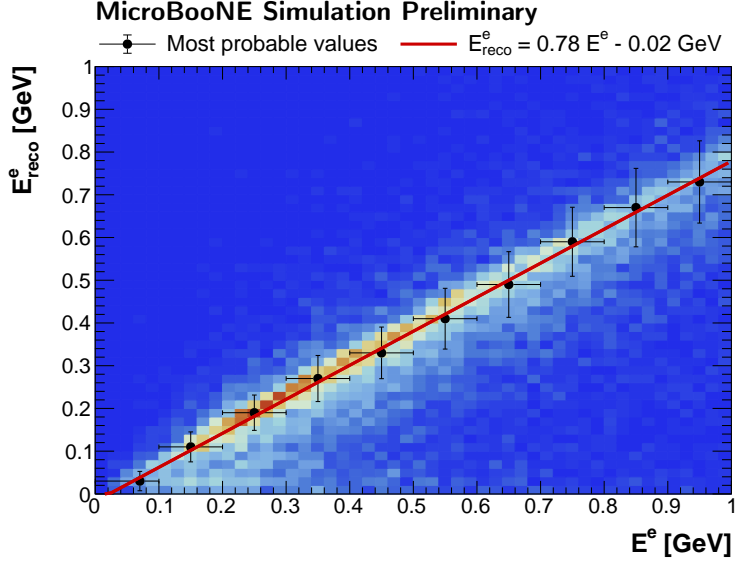
Figure 16: Bi-dimensional histogram of true electron energy E^e vs. reconstructed electron energy E^e_{reco}. The reconstructed electron energy is measured summing the energy of each hit associated to reconstructed showers produced by the simulated electron. The black points are obtained measuring the most probable value of the E^e_{reco} distribution for each E^e bin.

4.3 Single proton energy reconstruction and calibration

Proton energy reconstruction is obtained converting the reconstructed track length L into deposited energy using the proton stopping power in liquid argon, as tabulated in [22]. Liquid argon density ρ_{LAr} is assumed to be constant at 1.379 g/ml. Figure 17a shows the proton kinetic energy as a function of the range of the proton in liquid argon (measured as $L \times \rho_{LAr}$) .

The calibration constant has been obtained comparing the reconstructed energy of the proton with the true kinetic energy of the simulated proton, in a CC ν_e sample with only one proton in the final state. The true proton and the reconstructed tracks are required to be fully contained within the fiducial volume. Since protons are not minimum-ionizing particles, in the case of two or more tracks (*split tracks*) associated to the same proton, the reconstructed length of the tracks has been summed before calculating the corresponding kinetic energy. Figure 17b shows the calibration slope necessary to convert the proton reconstructed energy E^p_{reco} into true proton kinetic energy E^p. For each bin of the true proton energy, the most probable value of the corresponding proton reconstructed energy has been obtained with a Gaussian fit around the peak of the distribution. A linear fit of the data points gives:

$$E^p_{reco} = 0.99 \ E^p. \tag{5}$$

The energy of the track, corrected by the calibration factor is then defined as:

$$E^p_{deposited} = E^p_{reco}/0.99 \tag{6}$$
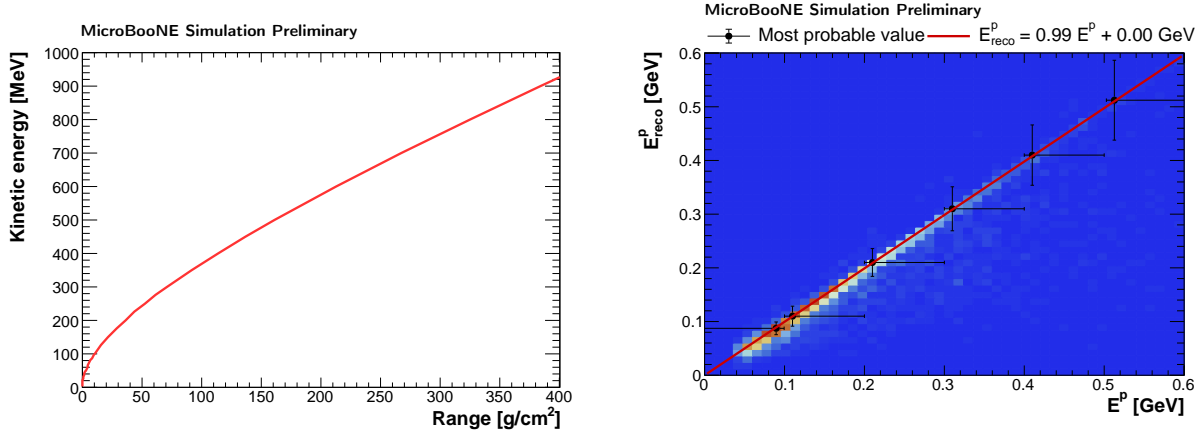
(a) Proton kinetic energy as a function of the range (b) Bi-dimensional histogram of true proton energy
of the proton in liquid argon. E^p vs. reconstructed proton energy E^p_{reco}.

Figure 17: The reconstructed proton energy is measured converting the reconstructed track length
L into deposited energy using the proton stopping power in liquid argon, as tabulated in
[22] (left). The calibration is calculated from a linear fit of the most probable values of
the E^p_{reco} distribution for each E^p bin (right).

4.4 Neutrino Energy Reconstruction

It is possible to compare the generated neutrino energy E_ν with the sum of the reconstructed
energies for shower-like ($E^e_{deposited}$) and track-like objects ($E^p_{deposited}$) for the selected ν_e CC0π-Np
events. This quantity $E_{deposited}$ is defined as:

$$E_{deposited} = \sum^{N_p} E^p_{deposited} + \sum^{N_e} E^e_{deposited}, \qquad (7)$$

where N_p is the number of reconstructed tracks and N_e is the number of reconstructed showers in
the event. For events where we have two or more shower-like objects and no track-like objects, only
one of the shower-like objects is chosen as proton candidate. In those cases we have $N_p = 1$ by
definition. The reconstructed energy does not include by definition particles that do not interact in
the liquid argon (such as neutrons) and charged particles with a kinetic energy below the detection
threshold. Figure 18 shows the calibration slope necessary to convert the the total reconstructed
energy $E_{deposited}$ into neutrino energy E_ν. The plot has been obtained using the ν_e CC0π-Np +
cosmic sample. A linear fit of the data points gives:

$$E_\nu = 0.86 \, E_{deposited}. \qquad (8)$$

This calibration factor is affected by several factors: among the others, the presence of regions
with unresponsive of missing wires can cause an underestimation of the deposited energy. In the
future, this effect can be limited by the use of the other two planes for calorimetric measurements.

However, due to uncertainties in the simulation of the interaction between the neutrino and the
argon nucleus, in this analysis we restrict ourselves to the quantity $E_{deposited}$, without trying to
measure the neutrino energy E_ν.
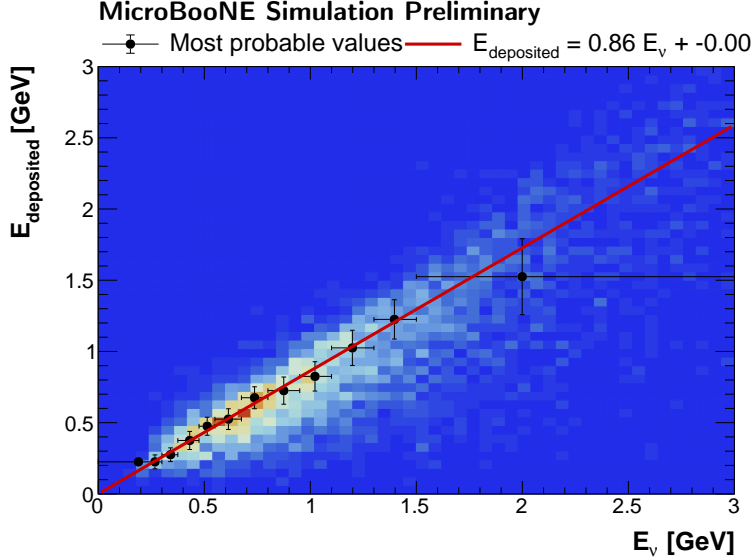
Figure 18: Bi-dimensional histogram of true neutrino energy E^ν vs. the total reconstructed energy $E_{deposited}$, corrected by the calibration factors. Black points are obtained measuring the most probable value of the $E_{deposited}$ distribution for each E_ν bin.

5 Validation

5.1 Side-bands checks

In this section we will study the agreement between data and Monte Carlo for selected samples orthogonal to our ν_e CC0π-Np signal. In order to validate our analysis, some of the background cuts described in Section 3.8 are inverted or removed in order to enhance different background components.

5.1.1 Photon-enhanced selection

It is possible to enhance the neutral-current component (defined as *beam intrinsic NC* in our analysis) by (1) inverting the cut on the shower dE/dx, (2) removing the requirement on the shower opening angle, and (3) removing the cut on the shower distance (see Figures 9a, 14a, 12a). The dE/dx of the most energetic shower must be within 3.2 MeV/cm and 5 MeV/cm to select electromagnetic cascades that were initiated by a photon. It also ensures that this photon-enhanced is orthogonal to the ν_e CC0π-Np selected sample. Removing the cut on the shower opening angle allows to include events where two photon showers from a $\pi^0 \to 2\gamma$ decay are reconstructed as a single object. The cut on the shower distance is removed to include events where the photon conversion is far from the neutrino interaction vertex. Thus, our final sample will mainly contain NC events, with some contamination of ν_μ CCπ^0 events where the muon track was tagged as a proton-like track.

Figure 19 shows the comparison between data and Monte Carlo for the reconstructed energy spectrum $E_{deposited}$ of the photon-enhanced event spectrum.
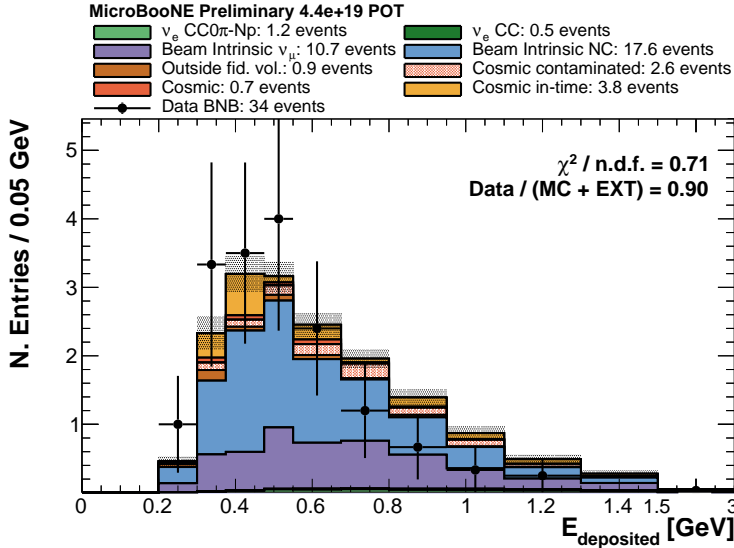
Figure 19: Reconstructed energy spectrum of the events selected with the photon-enhanced reverse cuts. The shaded area on top of the stacked histograms represent the statistical error, dominated by the size of the data off-beam sample.

5.1.2 CC ν_μ-enhanced reverse cuts

It is possible to enhance the presence of the CC ν_μ background (defined as *beam intrinsic ν_μ* in our analysis) by (1) requiring a minimum track length, (2) inverting the cut on the proton BDT (from BDT score > 0.1 to BDT score < 0.1), and (3) requiring that the event is selected by the external ν_μ CC-inclusive analysis [13] (see Figures 15a, 10a). Also in this case the CC ν_μ-enhanced sample will be orthogonal to the ν_e CC0π-Np selected sample. A CC ν_μ event has, by definition, a muon in the final state: as such, requiring a track length larger than 20 cm and inverting the cut on the proton BDT decreases our muon-rejection power. The goal of the external analysis is to select CC ν_μ events, so instead of vetoing those events as described in Section 3.7, we invert this requirement by allowing only these events.

Figure 20 shows the agreement between data and Monte Carlo for the reconstructed energy spectrum of the CC ν_μ-enhanced event spectrum.

5.2 Future Validation Studies

5.2.1 Cosmic-ray studies

In order to validate the cosmic-ray components of our selected events it is possible to compare simulated events with a CORSIKA cosmic ray producing a flash in the optical system during the beam-gate window and the data off-beam sample. In this way we will be able to check if the distributions of the variables we use (e.g. shower energy, shower dE/dx) show a good agreement between the simulation and a well-understood set of data events. It will help to validate the cosmic background components and also the energy and dE/dx reconstruction procedures.
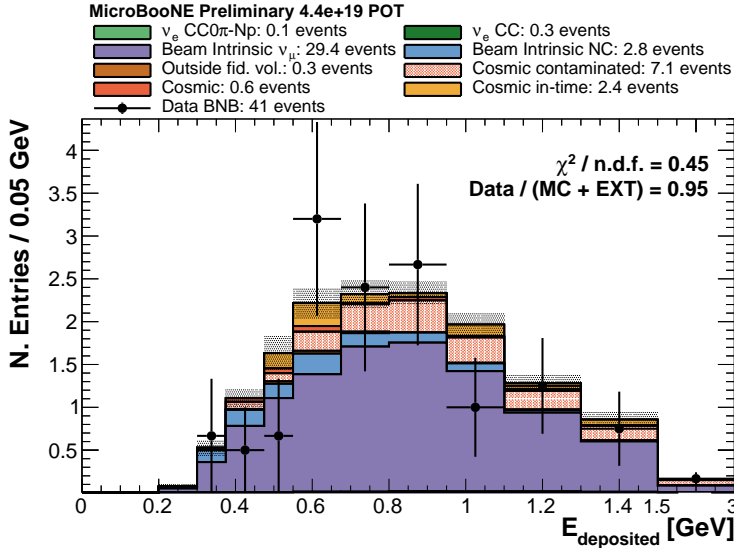
Figure 20: Reconstructed energy spectrum of the events selected with the CC ν_μ-enhanced reverse cuts. The shaded area on top of the stacked histograms represent the statistical error, dominated by the size of the data off-beam sample.

5.2.2 NuMI beam event studies

It is possible to run this analysis on the complementary NuMI dataset. The NuMI beam is created from 120 GeV protons hitting a carbon target, while the BNB is created from 8 GeV protons on a beryllium target. NuMI has also a higher beam intrinsic ν_e component than BNB (5% vs. 0.5%). Even though it is off-axis, MicroBooNE will still receive ~ 2500 ν_e interactions per year. As such, a study of the events selected in the NuMI dataset is of fundamental importance to validate the ν_e CC0π-Np selection algorithm.

6 Future Improvements

6.1 Cosmic tagging with the Cosmic-ray Tagger

As seen in Section 3.7, the dominant source of events passing the pre-selection is cosmic-ray interactions. The Cosmic-ray Tagger (CRT), described extensively in [23], offers several ways to reject these events at the pre-selection stage. First, a coincidence veto of in-time flashes in the PMTs and CRT would allow us to reject a significant background of in-time cosmic events. There is some danger that neutrino interactions are also vetoed by this coincidence, but that is unlikely for ν_e events - most particles that exit the TPC and can hit the CRT are muons.

Additionally, for events where an out-of-TPC neutrino interaction creates a flash in time with the beam, but a cosmic interaction is matched to that flash, the CRT can also be useful. TPC-to-CRT matching of muon tracks can mitigate this background by flagging a TPC Pandora neutrino candidate object, and allowing us to reject out-of-time cosmic rays matched to an in-time, out-of-TPC neutrino flash.

Cosmic-ray rejection is particularly important at low energy, where the component of events with

a selected cosmic ray in the signal sample is the largest one (Figure 3). For example, the shower energy distribution in Figure 8b shows a pile-up of cosmic-induced events at low energy and improved Michel and cosmic-ray tagging could help lowering the 50 MeV threshold.

The CRT was not used in this analysis because was not yet installed when the unblinded data sample analyzed here was recorded. At the moment, there are 5×10^{20} POT collected without the CRT and more than 4.5×10^{20} POT collected with the CRT. With the full approved running of MicroBooNE to 13.2×10^{20} POT, we anticipate we will collect 8.2×10^{20} POT with the CRT.

6.2 Reconstruction improvements

As shown in Section 3.6.1, the selection inefficiency depends on several factors. In particular, a better object reconstruction will allow to recover the events where reconstruction issues did not allow to satisfy the topology requirement (9.1% of the total) or in which we did not have any neutrino candidate (8.9%). Further improvements in reconstruction and selection can be made to reduce the cosmic contamination in the selected events (*cosmic contaminated* background).

In order to obtain a first estimate of the improvements that can be achieved with a better reconstruction, we measured the fraction of events selected after the cuts with a sub-sample of *perfectly classified* events. Here, by perfectly classified we mean that each proton (above the energy threshold) in the event was reconstructed as a track and the electron was reconstructed as shower.

A new set of algorithms has also been implemented in the CC ν_μ-inclusive analysis [13], which improves the cosmic-ray removal. The implementation of these algorithm also in this analysis will increase our selection efficiency, especially at low energies, where the events with a selected a cosmic-ray represent the largest component of the ν_e CC0π-Np sample, as shown in Figure 3.

6.3 Proton and electron particle identification

The current status of the analysis relies basically on the measured dE/dx of the reconstructed showers to identify the electron in the event and on the measured dQ/dx of the reconstructed tracks to identify the proton(s). An improvement in the shower clustering will directly cause an increase of the signal efficiency, since more electron showers will have a correctly measured dE/dx. Improvements in the proton identification are also underway: a more sophisticated algorithm, similar to the one described in [21], is currently being validated and it should sensibly increase the purity of our sample. In the majority of our ν_μ background events, a charged pion is reconstructed as a shower and identified as an electron or reconstructed as a track and identified as a proton. In the majority of the NC events, instead, the two photon showers from the $\pi^0 \rightarrow \gamma\gamma$ are reconstructed as one, or one does not get reconstructed. Both these backgrounds should therefore be considerably reduced by the future improvements.

6.4 Complementary Analyses

6.4.1 ν_μ Inclusive Selection

All MicroBooNE low-energy excess searches benefit greatly from the constraint of flux, cross sections, and perhaps detector systematics by performing a joint measurement of ν_μ and ν_e selections. In particular, the inclusive CC ν_μ cross-section measurement described in [13] also allows us to remove some ν_μ mis-reconstructed as ν_e CC0π-Np candidates. In addition, a CC0π-Np selection for ν_μ events will offer a strong constraint on the ν_e flux and cross-sections uncertainties.

6.4.2 Single Electron Inclusive Search

Since final state interactions of neutrinos on liquid argon are not yet completely understood, a complementary ν_e CC inclusive search is ongoing. The inclusive channel is expected to be less sensitive to uncertainties in the neutrino interaction models. By not requiring the presence of a proton higher sensitivities at low energy could be possible. The BNB ν_e CC inclusive search will also be compared with the ongoing NuMI ν_e CC inclusive measurement.

7 Conclusion

This analysis shows that it is possible to automatically select a sample with ν_e CC0π-Np events in a mainly ν_μ beam using the Pandora multi-algorithm pattern recognition. The current achieved reconstruction efficiency of these events is $(46.5 \pm 0.3)\%$.

The selection has been validated checking the agreement between data and Monte Carlo in a NC-enhanced sample and in a ν_μ-enhanced sample. The reconstructed energy spectrum of the selected events in orthogonal side-bands has been measured using a calorimetric-based technique for the shower-like objects and a length-based technique for the track-like objects.

We have already identified several improvements in the reconstruction of the objects in the TPC, in the background rejection, in the results of the complementary analyses, and with the inclusion of the CRT, which will allow us to further improve the selection of the ν_e CC0π-Np component, necessary to confirm or rule out the MiniBooNE low-energy excess.

References

[1] A. A. Aguilar-Arevalo *et al.* [MiniBooNE Collaboration], "Unexplained Excess of Electron-Like Events From a 1-GeV Neutrino Beam," Phys. Rev. Lett. **102** (2009) 101802 doi:10.1103/PhysRevLett.102.101802 `[arXiv:0812.2243 [hep-ex]]`.

[2] R. Acciarri *et al.*[MicroBooNE Collaboration], "Design and Construction of the Micro-BooNE Detector," JINST **12**, no. 02, P02017 (2017) doi:10.1088/1748-0221/12/02/P02017 `[arXiv:1612.05824 [physics.ins-det]]`.

[3] T. Katori [MiniBooNE and SciBooNE Collaborations], "Cross section analyses in MiniBooNE and SciBooNE experiments," AIP Conf. Proc. **1663** (2015) 020001 doi:10.1063/1.4919461 `[arXiv:1304.5325 [hep-ex]]`.

[4] R. Acciarri *et al.* [MicroBooNE Collaboration], "Noise Characterization and Filtering in the MicroBooNE Liquid Argon TPC," JINST **12**, no. 08, P08003 (2017) doi:10.1088/1748-0221/12/08/P08003 `[arXiv:1705.07341 [physics.ins-det]]`.

[5] J. S. Marshall and M. A. Thomson, "The Pandora Software Development Kit for Pattern Recognition", Eur. Phys. J. C **75**, no. 9, 439 (2015) doi:10.1140/epjc/s10052015-3659-3 `[arXiv:1506.05348 [physics.data-an]]`.

[6] R. Acciarri *et al.* [MicroBooNE Collaboration], "The Pandora multi-algorithm approach to automated pattern recognition of cosmic-ray muon and neutrino events in the MicroBooNE detector", `[arXiv:1708.03135 [physics.hep-ex]]`, accepted by Eur. Phys. J. C.

[7] C. Andreopoulos *et al.*, "The GENIE Neutrino Monte Carlo Generator," Nucl. Instrum. Meth. A **614** (2010) 87 doi:10.1016/j.nima.2009.12.009 `[arXiv:0905.2517 [hep-ph]]`.

[8] D. Heck *et al.*, "CORSIKA: A Monte Carlo code to simulate extensive air showers", 1998, `FZKA-6019`.

[9] R. Brun *et al.*, "GEANT Detector Description and Simulation Tool," doi:10.17181/CERN.MUHF.DMJ1

[10] E. D. Church, "LArSoft: A Software Package for Liquid Argon Time Projection Drift Chambers," `arXiv:1311.6774 [physics.ins-det]`.

[11] R. Acciarri *et al.* [MicroBooNE Collaboration], "Cosmic Shielding Studies at MicroBooNE", MICROBOONE-NOTE-1005-PUB, `http://microboone.fnal.gov/wp-content/uploads/MICROBOONE-NOTE-1005-PUB.pdf`

[12] R. Acciarri *et al.* [MicroBooNE Collaboration], "Measurement of cosmic-ray reconstruction efficiencies in the MicroBooNE LArTPC using a small external cosmic-ray counter," JINST **12**, no. 12, P12030 (2017) doi:10.1088/1748-0221/12/12/P12030 `[arXiv:1707.09903 [hep-ex]]`.

[13] R. Acciarri *et al.* [MicroBooNE Collaboration], "First Muon-Neutrino Charged-Current Inclusive Single and Double-Differential Cross Section Measurement for MicroBooNE Run 1 Data," MICROBOONE-NOTE-1045-PUB, *in preparation*.

[14] C. Adams *et al.* [MicroBooNE Collaboration], "Ionization Electron Signal Processing in Single Phase LArTPCs I. Algorithm Description and Quantitative Evaluation with MicroBooNE Simulation," submitted to JINST, [arXiv:1802.08709 [physics.ins-det].

[15] C. Adams *et al.* [MicroBooNE Collaboration], "Ionization Electron Signal Processing in Single Phase LArTPCs II. Data/Simulation Comparison and Performance in MicroBooNE," submitted to JINST, [arXiv:1804.02583 [physics.ins-det].

[16] R. Acciarri *et al.* [ArgoNeuT Collaboration], "First Observation of Low Energy Electron Neutrinos in a Liquid Argon Time Projection Chamber," Phys. Rev. D **95** (2017) no.7, 072005 doi:10.1103/PhysRevD.95.072005 [arXiv:1610.04102 [hep-ex]].

[17] A. Hocker *et al.*, "TMVA - Toolkit for Multivariate Data Analysis," PoS ACAT **2**, 040 (2007) [physics/0703039 [PHYSICS]].

[18] R. Acciarri *et al.* [MicroBooNE Collaboration], "Michel Electron Reconstruction Using Cosmic-Ray Data from the MicroBooNE LArTPC," JINST **12**, no. 09, P09014 (2017) doi:10.1088/1748-0221/12/09/P09014 [arXiv:1704.02927 [physics.ins-det]].

[19] Particle Data Group, "Atomic and nuclear properties of liquid argon (Ar)" http://pdg.lbl.gov/2012/AtomicNuclearProperties/MUON_ELOSS_TABLES/muonloss_289.pdf, retrieved Apr. 9, 2018

[20] M.E. Shibamura *et al.*, "Drift velocities of electrons, saturation characteristics of ionization and W-values for conversion electrons in liquid argon, liquid argon-gas mixtures and liquid xenon", Nucl. Instrumentation Meth., 131, (1975) p249

[21] R. Acciarri *et al.* [ArgoNeuT Collaboration], "A study of electron recombination using highly ionizing particles in the ArgoNeuT Liquid Argon TPC", JINST **8** (2013) P08005 558 [arXiv:1306.1712 [hep-ex]].

[22] M.J. Berger *et al.*, "ESTAR, PSTAR, and ASTAR: Computer Programs for Calculating Stopping-Power and Range Tables for Electrons, Protons, and Helium Ions (version 1.2.3)" (2005), http://physics.nist.gov/Star [2018, April 18]. National Institute of Standards and Technology, Gaithersburg, MD.

[23] M. Auger *et al.*, "A Novel Cosmic Ray Tagger System for Liquid Argon TPC Neutrino Detectors," Instruments **1**, no. 1, 2 (2017) doi:10.3390/instruments1010002 [arXiv:1612.04614 [physics.ins-det]].